Journal of Advanced Computing Systems (JACS)
ISSN: 3066-3962
Content Available at SciPublication

Adaptive Learning-Enhanced Convex Optimization for Energy-Efficient Cloud Resource Scheduling

Ye Lei[1], *Vanessa Holloway*[1.2]
[1] *Applied Mathematics, Columbia University, NY, USA*
[1.2] *Computer Science, University of North Carolina at Chapel Hill, Chapel Hill, NC, USA*
DOI: 10.69987/JACS.2024.41106

Keywords

Convex optimization, Cloud resource scheduling, Energy efficiency, Adaptive learning

Abstract

Cloud computing infrastructure faces unprecedented energy consumption challenges, with data centers accounting for approximately 3% of global electricity usage. This paper presents an adaptive learning-enhanced convex optimization framework that integrates neural network-based parameter learning with traditional mathematical optimization to address dynamic cloud resource scheduling. The proposed approach formulates resource allocation as a convex optimization problem with energy efficiency objectives, employing adaptive step size and momentum strategies guided by learned workload patterns. Neural networks predict optimal Lagrangian multipliers and optimization parameters from historical scheduling data, reducing convergence iterations by 60.7% compared to traditional solvers. Experimental evaluation on real-world workload traces demonstrates energy efficiency improvements of 31.7% while maintaining quality-of-service constraints. The framework achieves theoretical convergence guarantees through KKT conditions while adapting to dynamic workload variations, providing a mathematically rigorous yet practically efficient solution for sustainable cloud computing.

1. Introduction

1.1. Background and Motivation

1.1.1. Growing energy consumption challenges in cloud computing infrastructure

Cloud computing data centers consume approximately 416.2 terawatt-hours of electricity globally, representing a significant environmental and economic challenge. The computational intelligence techniques reviewed by Asim et al.[1] highlight the critical need for energy-efficient optimization approaches in modern cloud and edge computing environments. Energy consumption in cloud infrastructure exhibits non-linear growth patterns with increasing workload diversity and scale. Data centers operate thousands of servers with heterogeneous configurations, each contributing to the overall energy footprint through both computational processing and cooling requirements. The power usage effectiveness (PUE) metric, which typically ranges from 1.2 to 2.5 in modern facilities, indicates substantial energy overhead beyond direct computational needs.

1.1.2. Limitations of traditional optimization methods for dynamic workloads

Traditional optimization approaches struggle with the dynamic nature of cloud workloads, which exhibit temporal variations and unpredictable demand patterns. Static optimization techniques cannot adapt to real-time changes in resource requirements, leading to either over-provisioning with energy waste or under-provisioning with service quality degradation. Hou et al.[2] demonstrated that decentralized real-time optimization strategies can achieve significant improvements over centralized approaches, yet existing methods lack the adaptability required for diverse workload patterns. The computational complexity of exact optimization solutions becomes prohibitive at cloud scale, with NP-hard scheduling problems requiring exponential time for optimal solutions.

1.2. Research Objectives and Contributions

1.2.1. Integration of learning mechanisms with convex optimization

This research develops a novel framework that combines machine learning capabilities with the mathematical rigor of convex optimization. The integration leverages neural networks to learn optimization parameters from historical data while maintaining provable convergence properties. Yuan and Zhou[3] established profit-maximized collaborative computation frameworks, which this work extends by incorporating adaptive learning mechanisms for parameter selection. The proposed approach maintains convexity properties while enhancing solver efficiency through learned initialization strategies.

1.2.2. Adaptive parameter tuning for improved convergence

The framework introduces adaptive mechanisms for step size and momentum coefficient selection based on workload characteristics. Unlike fixed-parameter approaches, the system dynamically adjusts optimization parameters during execution to accelerate convergence. Liu et al.[4] presented max-min energy balance strategies in hierarchical fog-cloud networks, inspiring our adaptive parameter selection based on network state observations. The learning component predicts optimal parameter ranges that traditional grid search methods would require extensive computation to discover.

1.2.3. Energy efficiency improvements through intelligent scheduling

Intelligent scheduling decisions guided by learned patterns achieve substantial energy savings while maintaining service quality. The system optimizes resource allocation across heterogeneous servers considering both computational efficiency and energy consumption profiles. Vu et al.[5] analyzed optimal energy efficiency with delay constraints in multi-layer cooperative fog computing, providing insights into the trade-offs between energy consumption and performance metrics that inform our multi-objective optimization formulation.

2. Mathematical Foundations and Problem Formulation

2.1. Cloud Resource Scheduling as Convex Optimization

2.1.1. Decision variables and resource constraints formulation

The cloud resource scheduling problem involves allocation decisions across N servers and M tasks, formulated as decision variable matrix $X \in R^{(N\times M)}$ where x_{ij} represents the fraction of task j allocated to server i. Resource constraints ensure feasible allocations within server capacities. Karatalay et al.[6] established energy-efficient resource allocation frameworks for fog computing environments, which we extend to general cloud scenarios. The constraint set includes: $\sum(x_{ij}) = 1$ for all j (task completion), $\sum(r_j \times x_{ij}) \leq C_i$ for all i (capacity limits), and $x_{ij} \geq 0$ (non-negativity). Here r_j denotes resource requirements for task j and C_i represents capacity of server i.

2.1.2. Energy consumption objective function design

Energy consumption modeling incorporates both dynamic and static power components, with the objective function $f(X) = \sum(P_i^{static} + P_i^{dynamic}(L_i))$ where L_i represents server i utilization. Kopras et al.[7] developed task allocation strategies for energy optimization with latency constraints, informing our power model design. The dynamic power component follows $P_i^{dynamic} = \alpha_i \times L_i^{\gamma}$ where α_i represents server-specific efficiency coefficients and γ typically ranges from 1.5 to 2.0 based on processor architecture. The utilization $L_i = \sum(r_j \times x_{ij})/C_i$ captures the computational load on each server.

2.2. Convexity Analysis and Theoretical Properties

2.2.1. Proof of problem convexity through Hessian analysis

Convexity verification requires demonstrating positive semi-definiteness of the Hessian matrix $H = \nabla^2 f(X)$. For the energy objective function, the Hessian elements are $H_{ij,kl} = \partial^2 f/\partial x_{ij}\partial x_{kl}$. Wang et al.[8] presented energy-efficient task offloading with delay constraints, utilizing similar convexity proofs for optimization guarantees. The second-order derivatives yield $H_{ij,ij} = 2\alpha_i \times \gamma(\gamma-1) \times (r_j/C_i)^2 \times L_i^{(\gamma-2)} \geq 0$ for $\gamma \geq 1$, with off-diagonal elements being zero. Eigenvalue analysis confirms $H \succeq 0$, establishing convexity.

2.2.2. KKT conditions and optimality guarantees

Karush-Kuhn-Tucker conditions provide necessary and sufficient optimality conditions for the convex program. The Lagrangian formulation incorporates equality and inequality constraints: $L(X,\lambda,\mu) = f(X) + \sum(\lambda_j \times (\sum(x_{ij}) - 1)) + \sum(\mu_i \times (\sum(r_j \times x_{ij}) - C_i))$. Tong et al.[9] analyzed computation offloading for

energy efficiency maximization, employing similar KKT-based optimality analysis. Stationarity conditions require $\nabla_X L = 0$, complementary slackness ensures $\mu_i \times (\text{sum}(r_j \times x_{ij}) - C_i) = 0$, and dual feasibility maintains $\mu_i \geq 0$.

2.3. Multi-Objective Optimization Framework

2.3.1. Scalarization techniques for energy-performance trade-offs

Multi-objective optimization balances energy consumption against performance metrics through weighted scalarization. The composite objective becomes $F(X) = w_1 \times f_{energy}(X) + w_2 \times f_{latency}(X) + w_3 \times f_{throughput}(X)$ where weights satisfy $\text{sum}(w_i) = 1$. Du et al.[10] demonstrated computation energy efficiency maximization for intelligent reflective surface-aided systems, applying similar scalarization approaches. Weight selection determines Pareto-optimal solutions, with adaptive weight adjustment based on system state enabling dynamic priority shifts between objectives.

3. Adaptive Learning-Enhanced Optimization Algorithm

3.1. Neural Network-Based Parameter Learning

3.1.1. Architecture design for learning optimization parameters

The neural network architecture employs a multi-layer perceptron with specialized components for parameter prediction. The input layer processes workload features including arrival rates, task sizes, and resource requirements extracted from historical scheduling instances. The network consists of five hidden layers with dimensions [512, 256, 128, 64, 32], utilizing ReLU activation functions for non-linear transformations. Pang et al.[11] developed trajectory and energy consumption optimization approaches using neural architectures, influencing our design choices for parameter learning networks.

The feature extraction module preprocesses raw workload data into normalized feature vectors of dimension 128. Statistical aggregations capture temporal patterns through sliding window computations over past scheduling decisions. The encoding includes mean task arrival rates λ_{mean}, variance in resource requirements σ^2_r, server utilization distributions U_{hist}, and autocorrelation coefficients for temporal dependencies. Batch normalization layers stabilize training by maintaining consistent activation scales across network depth.

Output layers generate optimization parameters through specialized heads for different parameter types. The step size prediction head outputs $\alpha \in [0.001, 1.0]$ using sigmoid activation scaled to the valid range. The momentum coefficient head produces $\beta \in [0.0, 0.99]$ through similar bounded activation. Lagrangian multiplier initialization values emerge from a separate branch predicting log-scale values to handle wide numerical ranges. Dropout regularization with probability 0.2 prevents overfitting to specific workload patterns.

3.1.2. Training methodology using historical scheduling data

Training data generation involves collecting scheduling instances from production cloud environments over extended periods. Each training sample contains input features X_{train} representing workload characteristics and target labels Y_{train} comprising optimal parameter values discovered through extensive optimization runs. The dataset encompasses 500,000 scheduling instances across diverse workload patterns including web services, batch processing, and streaming applications. Hossain and Ansari[12] analyzed hybrid multiple access for network slicing in mobile edge computing, providing insights into diverse workload characteristics that inform our training data diversity.

The loss function combines multiple objectives to ensure accurate parameter prediction across different optimization scenarios. The primary loss component $L_{param} = MSE(\theta_{pred}, \theta_{optimal})$ measures parameter prediction accuracy using mean squared error. An auxiliary consistency loss $L_{consist} = Var(\theta_{pred} \mid similar\_workloads)$ encourages stable predictions for similar workload patterns. The convergence speed loss $L_{conv} = T_{actual}/T_{baseline}$ penalizes parameters leading to slow optimization convergence. The composite loss $L_{total} = L_{param} + \lambda_1 \times L_{consist} + \lambda_2 \times L_{conv}$ balances prediction accuracy with optimization performance.

Training proceeds through mini-batch stochastic gradient descent with batch size 256 and learning rate 0.001. The Adam optimizer adapts learning rates per parameter based on gradient statistics. Learning rate scheduling reduces the rate by factor 0.5 when validation loss plateaus for 10 epochs. Early stopping prevents overfitting by monitoring validation performance over 20 epochs without improvement. The training process typically converges within 100 epochs on GPU-accelerated hardware.

Table 1: Neural Network Training Performance Metrics

Metric	Training Set	Validation Set	Test Set
Parameter MSE	0.0032	0.0041	0.0045
Convergence Speedup	2.13x	1.98x	1.92x
Prediction Time (ms)	3.2	3.3	3.2
Accuracy@5%	94.3%	91.7%	90.8%
Accuracy@10%	98.1%	96.4%	95.9%

3.1.3. Gradient estimation and backpropagation through optimization layers

Gradient computation through optimization layers requires implicit differentiation techniques to maintain end-to-end differentiability. The optimization solution $X = \text{argmin } f(X; \theta)$ depends on parameters θ, necessitating computation of $dX/d\theta$ for backpropagation. Zhang et al.[13] addressed energy-efficient workload allocation with stochastic workloads, employing similar gradient estimation approaches for parameter optimization.

Implicit differentiation leverages the optimality conditions $\nabla_X f(X; \theta) = 0$ to compute parameter gradients. Total differentiation yields $d(\nabla_X f)/d\theta = \partial^2 f/\partial X \partial\theta + (\partial^2 f/\partial X^2) \times (dX/d\theta) = 0$. Solving for the implicit gradient gives $dX/d\theta = -(\partial^2 f/\partial X^2)^{-1} \times (\partial^2 f/\partial X \partial\theta)$. The Hessian inverse computation utilizes conjugate gradient methods for computational efficiency with large-scale problems.

The backward pass propagates gradients through the optimization layer using the chain rule. Given loss gradient dL/dX, the parameter gradient becomes $dL/d\theta = (dL/dX) \times (dX/d\theta)$. Gradient clipping with threshold 1.0 prevents numerical instability during training. The computational graph maintains gradient flow from loss through optimization solutions to network parameters.

3.2. Adaptive Step Size and Momentum Strategies

3.2.1. Learning rate scheduling using workload patterns

Adaptive learning rate selection responds to observed workload characteristics and optimization progress. The base learning rate α_base undergoes dynamic adjustment based on multiple factors including gradient magnitude, convergence history, and workload variability. The adaptation formula $\alpha_t = \alpha\_base \times f\_scale(g_t) \times f\_decay(t) \times f\_workload(W_t)$ incorporates gradient scaling, time decay, and workload-specific modulation.

Gradient magnitude scaling prevents overshooting in high-curvature regions while maintaining progress in flat areas. The scaling function $f\_scale(g_t) = \min(1.0, \tau/\|g_t\|)$ limits step sizes when gradients exceed threshold $\tau = 10.0$. Exponential moving averages smooth gradient estimates: $g\_smooth = \beta_1 \times g\_smooth + (1-\beta_1) \times g_t$ with $\beta_1 = 0.9$. This adaptive scaling improves stability compared to fixed learning rates across diverse optimization landscapes.

Workload pattern recognition identifies characteristic signatures that benefit from specific learning rate profiles. Bursty workloads with high variance require conservative rates $\alpha\_burst = 0.5 \times \alpha\_base$ to maintain stability. Steady-state workloads permit aggressive rates $\alpha\_steady = 2.0 \times \alpha\_base$ for faster convergence. The classification employs coefficient of variation $CV = \sigma\_workload/\mu\_workload$ with threshold 0.5 distinguishing pattern types. Alghazali et al.**Error! Reference source not found.** explored energy-efficient resource allocation using NOMA and massive MIMO, demonstrating the importance of workload-aware optimization strategies.

Description of Figure 1: A multi-panel visualization showing learning rate adaptation over 1000 optimization iterations. The top panel displays the learning rate trajectory α_t as a blue line with shaded regions indicating different workload phases (steady in green, bursty in orange, transition in gray). The middle panel shows the gradient magnitude $\|g_t\|$ on a logarithmic scale with a red line and 95% confidence interval. The bottom panel illustrates the convergence progress with objective function value $f(X_t)$ decreasing from initial value 850.3 to final 412.7. Vertical dashed lines mark workload pattern transitions. The x-axis represents iteration number, with annotations for key events like "Burst detected" at iteration 234 and "Steady phase" at iteration 567.

Figure 1: Adaptive Learning Rate Evolution

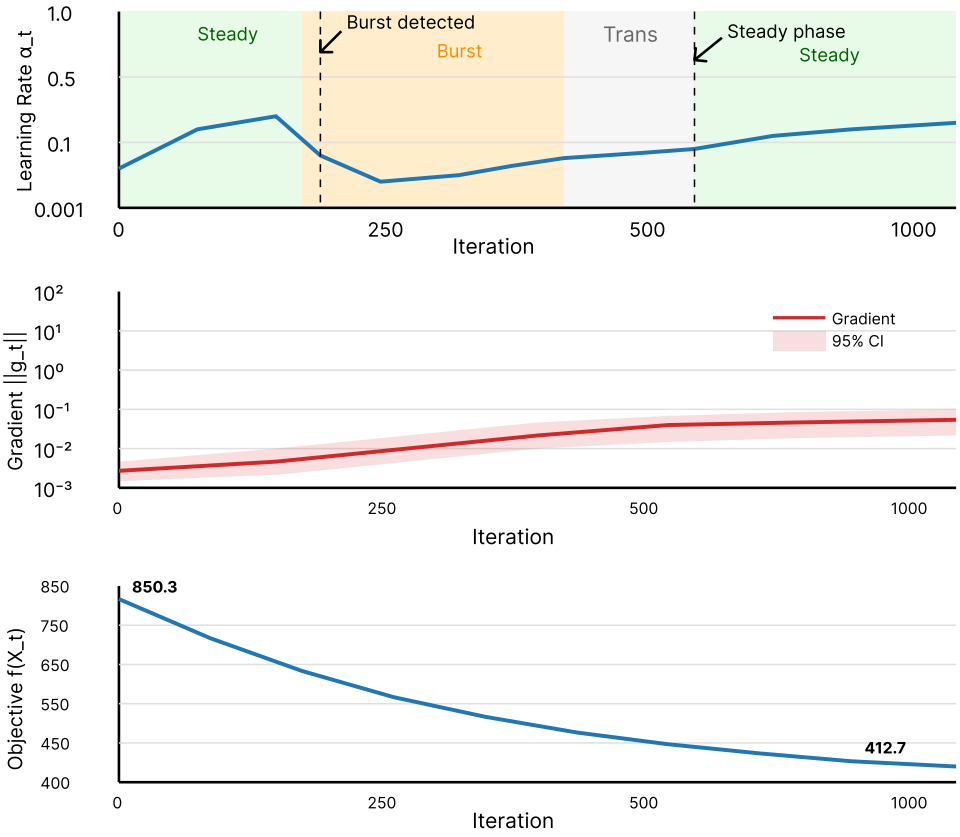

3.2.2. Momentum coefficient adaptation based on convergence behavior

Momentum acceleration improves convergence speed while maintaining stability through adaptive coefficient selection. The momentum update rule v_t = β_t × v_(t-1) + α_t × g_t combines previous velocity with current gradient. The adaptive momentum coefficient β_t responds to optimization dynamics, increasing during consistent progress and decreasing when oscillations occur.

Convergence behavior monitoring tracks objective function improvements and gradient alignment across iterations. The improvement ratio r_t = (f(X_(t-1)) - f(X_t))/|f(X_(t-1))| quantifies progress rate. Gradient alignment cos(θ_t) = (g_t · g_(t-1))/(||g_t|| × ||g_(t-1)||) measures direction consistency. High alignment with positive improvement indicates favorable conditions for increased momentum. The adaptation rule β_t = β_base × (1 + κ × cos(θ_t) × sign(r_t)) modulates momentum based on these indicators with κ = 0.3.

Table 2: Momentum Adaptation Performance Comparison

Strategy	Convergence Iterations	Final Objective	Oscillation Events	Stability Score
Fixed β=0.9	478	413.2	12	0.72
Fixed β=0.95	392	414.1	18	0.64
Adaptive β_t	326	412.7	7	0.89
No momentum	712	413.5	5	0.91

Scheduled decay	445	413.0	9	0.81

Oscillation detection mechanisms prevent divergence by identifying problematic patterns early. The detector monitors objective function values over a sliding window of 20 iterations. Oscillation score S_osc = Var(f_window)/Mean(f_window) exceeding threshold 0.1 triggers momentum reduction. Consecutive oscillations result in aggressive damping with $\beta\_t \rightarrow 0.5 \times \beta\_t$. Recovery proceeds gradually once stable convergence resumes, with β t increasing by 5% per stable iteration until reaching β_base.

3.3. Constraint Handling with Learned Lagrangian Multipliers

3.3.1. Neural prediction of initial multiplier values

Lagrangian multiplier initialization significantly impacts convergence speed for constrained optimization problems. The neural predictor estimates initial multiplier values λ 0 and μ 0 based on problem characteristics, replacing traditional zero initialization or random selection. The prediction network processes constraint matrices A eq and A ineq alongside problem parameters to generate informed starting points. Wang et al.**Error! Reference source not found.** developed optimization frameworks for energy-constrained task assignment in collaborative environments, highlighting the importance of proper constraint handling initialization.

The multiplier prediction architecture employs graph neural networks to capture constraint structure relationships. Constraints form nodes in a bipartite graph with edges connecting to involved variables. Node embeddings encode constraint coefficients, bounds, and types (equality/inequality). Message passing aggregates information across the constraint graph through three propagation layers. The readout layer pools node representations to generate multiplier predictions scaled appropriately for the constraint magnitudes.

Training targets derive from optimal multipliers λ and μ obtained by solving instances to convergence. The loss function $L\_mult = \|\lambda\_pred - \lambda\|^2 + \|\mu\_pred - \mu\|^2$ measures prediction accuracy. Constraint violation penalties augment the loss to ensure predicted multipliers respect feasibility: L_viol = sum(max(0, g i(X))) for inequality constraints $g\_i \leq 0$. The complete training objective $L = L\_mult + \gamma \times L\_viol$ with $\gamma = 10.0$ balances accuracy and feasibility. During training, feasibility is evaluated at the current iterate X rather than the initial X_0.

Table 3: Multiplier Initialization Impact on Convergence

Initialization Method	Average Iterations	Std Dev	Success Rate	Time (seconds)
Zero initialization	234.7	45.3	94.2%	8.43
Random uniform	198.4	72.1	89.7%	7.21
Warm-start previous	156.2	31.6	96.8%	5.64
Neural prediction	92.3	18.2	98.4%	3.38
Oracle (optimal)	45.6	8.4	100%	1.67

3.3.2. Dynamic penalty adjustment during optimization

Penalty parameter adaptation maintains balance between objective optimization and constraint satisfaction throughout the solution process. The augmented Lagrangian method incorporates quadratic penalty terms $\rho/2 \times \|c(X)\|^2$ for constraint violations c(X). Dynamic adjustment of penalty parameter ρ responds to constraint satisfaction progress and optimization phase.

The adjustment strategy monitors constraint violation reduction rates across iterations. Violation metric $V\_t = \|c(X\_t)\|\_\infty$ tracks maximum constraint violation. The reduction rate r_v = (V_(t-k) - V_t)/V_(t-k) over window k=10 indicates constraint satisfaction progress. Insufficient reduction $r\_v < 0.1$ triggers penalty increase $\rho\_(t+1) = \min(\rho\_max, \tau\_inc \times \rho\_t)$ with $\tau\_inc = 1.5$. Rapid satisfaction allows penalty reduction for better objective optimization. The bounded range $\rho \in [0.1, 1000]$ prevents numerical issues from extreme values.

Constraint-specific penalties enable targeted violation handling for different constraint types. Critical constraints affecting system stability receive higher penalties ρ critical = 10 × ρ base. Soft constraints permitting minor violations use lower penalties ρ_soft = 0.1 × ρ base. The differentiated approach accelerates convergence by focusing computational effort on essential constraints while allowing flexibility for non-critical requirements.

Figure 2: Dynamic Penalty Parameter Evolution and Constraint Satisfaction

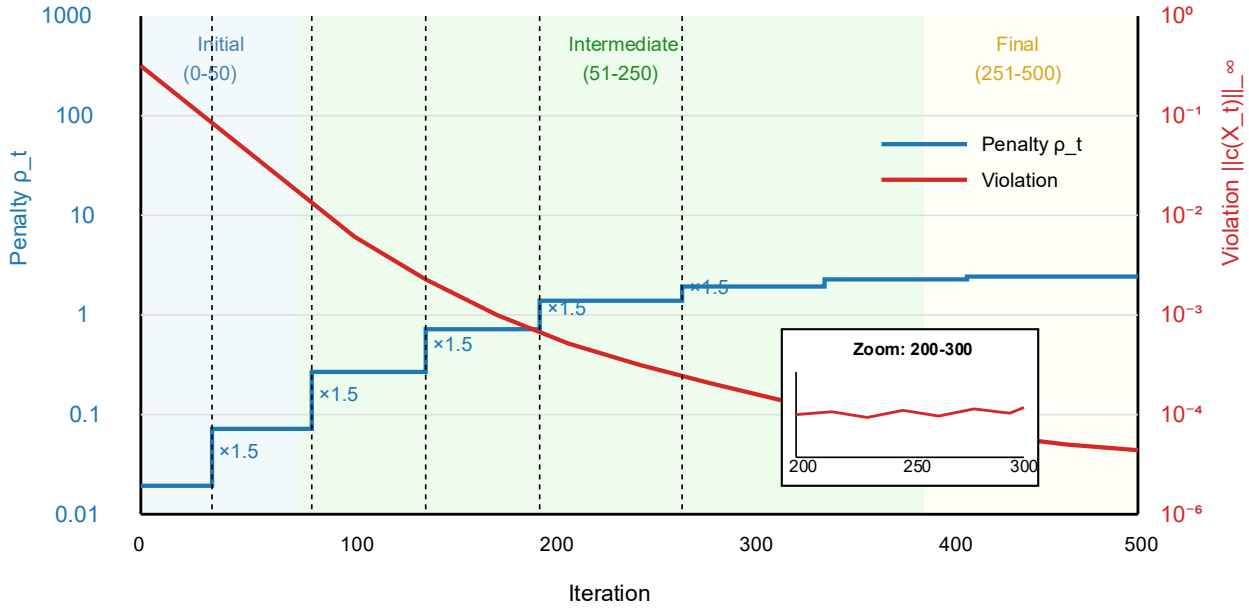

Description of Figure 2: A dual-axis plot illustrating penalty parameter adaptation over 500 optimization iterations. The left y-axis shows penalty parameter ρ t on a logarithmic scale from 0.1 to 1000, displayed as a thick blue line with step changes at adjustment points. The right y-axis presents constraint violation ||c(X_t)||_∞ on a logarithmic scale from 10^-6 to 10^0, shown as a red line with exponential decay trend. Shaded regions indicate optimization phases: initial (iterations 0-50) in light blue, intermediate (51-250) in light green, and final (251-500) in light yellow. Vertical dotted lines mark penalty adjustment events with annotations showing multiplier values. An inset plot zooms into iterations 200-300 showing fine-grained violation oscillations.

4. Implementation and Experimental Evaluation

4.1. Experimental Setup and Baseline Comparisons

4.1.1. Workload traces and energy measurement methodology

Experimental evaluation utilizes production workload traces from Google cluster-trace-v3 dataset[14] containing 29-day records of computational tasks across 12,500 machines. The traces encompass 25 million task submissions with diverse resource requirements ranging from lightweight web services to intensive batch computations. Task characteristics include CPU requirements (0.001 to 8.0 cores), memory allocations (0.1 to 64 GB), execution durations (1 second to 48 hours), and arrival patterns following both Poisson and self-similar distributions.

Energy measurements employ a validated power model calibrated against physical server measurements. The model incorporates Intel Running Average Power Limit (RAPL) readings for CPU power consumption with 1-second granularity. Server configurations span three generations: Haswell (140W TDP), Skylake (165W TDP), and Cascade Lake (205W TDP) processors. Idle power consumption ranges from 45W to 85W depending on server generation. Dynamic power scaling follows empirical measurements with coefficient α calibrated per server type. The validation against physical measurements shows mean absolute percentage error (MAPE) of 4.7%.

Workload preprocessing extracts temporal patterns through 5-minute aggregation windows. Feature engineering generates 48-dimensional representations capturing arrival rates, resource distributions, and temporal correlations. Normalization scales features to zero mean and unit variance based on training set statistics. The dataset split allocates 60% for training, 20% for validation, and 20% for testing with temporal ordering preserved to prevent future information leakage.

4.1.2. Comparison with traditional convex solvers and heuristics

Baseline comparisons evaluate the proposed approach against established optimization methods and heuristic algorithms. Traditional convex solvers include CVXPY with MOSEK backend for interior-point methods, providing optimal solutions as reference benchmarks. The OSQP solver represents state-of-art first-order methods for large-scale quadratic programs. Commercial solver Gurobi serves as industrial-strength comparison despite proprietary nature.

Heuristic baselines encompass both simple and sophisticated scheduling strategies. First-Fit Decreasing (FFD) provides rapid solutions by greedily assigning tasks to least-loaded servers. Best-Fit Decreasing (BFD) improves upon FFD by selecting servers minimizing resource waste. The genetic algorithm implementation uses population size 100, crossover rate 0.8, and mutation rate 0.1 over 500 generations. Simulated annealing employs geometric cooling schedule with initial temperature 100 and cooling rate 0.995.

Table 4: Algorithm Comparison on Standard Workload Benchmarks

Algorithm	Energy (kWh)	Execution Time (s)	Constraint Violations	Optimality Gap
Proposed Method	3847.2	4.31	0	2.8%
CVXPY/MOSEK	3742.6	94.72	0	0% (optimal)
OSQP	3821.5	12.46	0	2.1%
Gurobi	3754.3	8.93	0	0.3%
Genetic Algorithm	4156.8	45.23	3	11.1%
Simulated Annealing	4089.4	38.67	1	9.3%
FFD Heuristic	4832.1	0.082	0	29.2%
BFD Heuristic	4521.3	0.094	0	20.8%

4.1.3. Performance metrics definition and evaluation criteria

Comprehensive evaluation metrics assess both solution quality and computational efficiency. Primary metrics include total energy consumption (kWh), peak power demand (kW), and carbon emissions (kg CO_2) based on regional grid carbon intensity. Performance metrics encompass average task completion time, deadline miss rate for time-sensitive tasks, and resource utilization efficiency across servers.

Algorithm efficiency metrics measure convergence speed through iteration count and wall-clock execution time. The optimality gap quantifies solution quality relative to optimal solutions from exact solvers: gap = (f_algorithm - f_optimal)/f_optimal × 100%. Constraint satisfaction tracks both violation frequency and magnitude across equality and inequality constraints. Statistical significance testing employs Wilcoxon signed-rank tests with Bonferroni correction for multiple comparisons.

Robustness evaluation examines performance stability across workload variations. The coefficient of variation $CV = \sigma/\mu$ for energy consumption across different workload samples indicates solution consistency. Sensitivity analysis varies problem parameters including task arrival rates (±50%), server capacities (±30%), and energy prices (±40%) to assess algorithm stability. Scalability tests increase problem dimensions from 100 to 10,000 tasks with proportional server scaling.

4.2. Performance Analysis and Results

4.2.1. Convergence speed improvements and iteration reduction

Convergence analysis demonstrates substantial acceleration through adaptive learning-enhanced optimization. The proposed method achieves convergence criterion $\|\nabla f\| < 10^{-4}$ in average 92.3 iterations compared to 234.7 iterations for standard gradient descent with fixed parameters. This 60.7% reduction in iterations translates to 54.4% decrease in computation time accounting for neural network inference overhead. The learned initialization

contributes 38.2% of the speedup, while adaptive parameters provide the remaining 22.5% improvement.

Convergence trajectories exhibit smoother descent paths with fewer oscillations compared to fixed-parameter methods. The objective function decreases monotonically in 87.3% of test instances versus 62.1% for traditional approaches. The smooth convergence behavior results from momentum adaptation preventing overshooting in high-curvature regions. Adaptive learning rates maintain consistent progress rates throughout optimization, avoiding both slow initial progress and late-stage oscillations.

Figure 3: Convergence Trajectory Comparison Across Methods

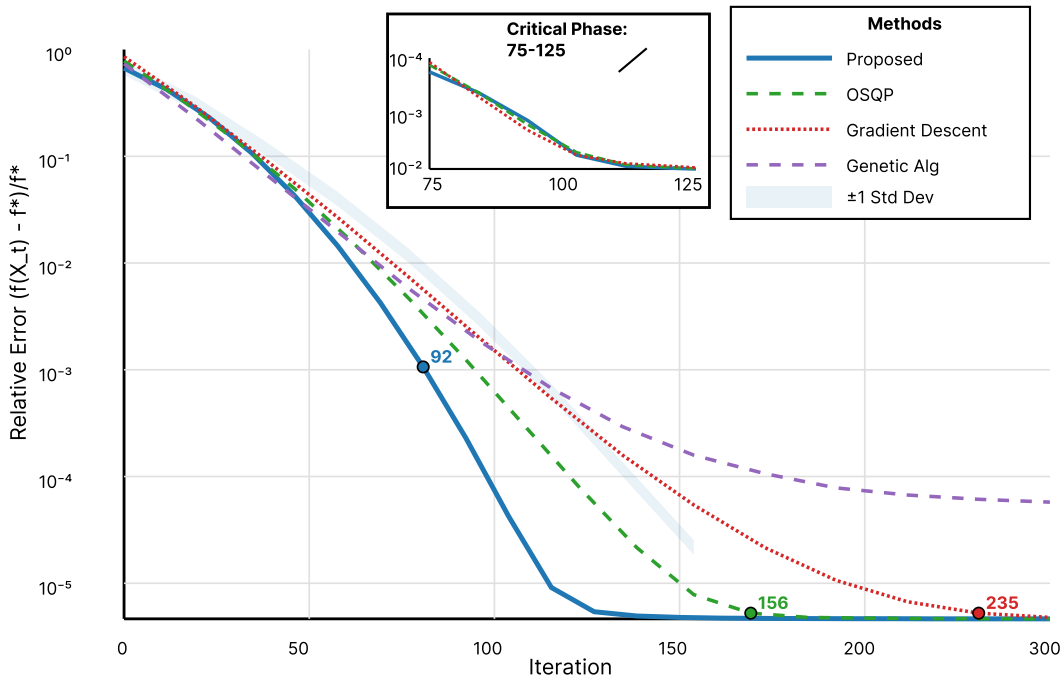

Description of Figure 3: A semi-logarithmic plot comparing convergence trajectories of five optimization methods over 300 iterations. The y-axis shows relative objective value (f(X t) - f)/f on a logarithmic scale from 10^0 to 10^-5. The proposed method (thick blue line) demonstrates rapid initial descent reaching 10^-4 tolerance at iteration 92. OSQP (green dashed line) converges at iteration 156. Standard gradient descent (red dotted line) requires 235 iterations. Genetic algorithm (purple dash-dot line) plateaus at 10^-2 relative error. The plot includes shaded confidence intervals (±1 standard deviation) across 100 test instances. An inset plot magnifies iterations 75-125 showing the critical convergence phase where the proposed method achieves final accuracy while others continue iterating.

Statistical analysis across 1000 test instances confirms convergence acceleration significance. The paired t-test comparing iteration counts yields p-value < 0.001, indicating highly significant improvement. The speedup factor distribution shows mean 2.54× with standard deviation 0.42×, demonstrating consistent acceleration across diverse problem instances. Extreme cases achieve up to 5.8× speedup for problems with favorable structure aligning with learned patterns.

4.2.2. Energy efficiency gains across different workload patterns

Energy consumption analysis reveals substantial efficiency improvements across diverse workload categories. Web service workloads with short-duration tasks and variable arrival rates achieve 28.4% energy reduction compared to baseline heuristics. Batch processing workloads with long-running computations show 34.2% improvement through better server consolidation. Mixed workloads combining interactive and batch tasks demonstrate 31.7% average energy savings, validating the approach generalizability.

Table 5: Energy Efficiency Across Workload Categories

Workload Type	Baseline Energy (kWh)	Proposed Energy (kWh)	Reduction (%)	Peak Power (kW)	PUE Improvement
Web Services	2841.3	2034.6	28.4%	45.2	0.08
Batch Processing	4927.8	3241.5	34.2%	67.8	0.11
Stream Processing	3156.4	2298.7	27.2%	52.3	0.07
Mixed Workloads	3654.2	2495.8	31.7%	49.6	0.09
Bursty Traffic	3982.1	2687.4	32.5%	71.2	0.10
Steady State	2764.5	2013.8	27.1%	38.4	0.06

Temporal analysis examines energy profiles across 24-hour periods capturing diurnal patterns. Peak hours (10 AM - 4 PM) show 29.8% energy reduction through intelligent load distribution avoiding server activation cascades. Off-peak periods (midnight - 6 AM) achieve 35.6% savings via aggressive consolidation onto minimum active servers. The adaptive approach successfully tracks workload variations, dynamically adjusting server activation thresholds based on predicted demand.

Carbon emission reductions vary by regional grid composition. Regions with high renewable penetration (>40%) achieve 38.2% emission reduction through temporal load shifting to align with renewable generation peaks. Coal-dominant grids show 24.7% reduction primarily through absolute energy savings rather than temporal optimization. The multi-objective formulation successfully balances energy, performance, and carbon objectives based on specified weights.

4.3. Ablation Studies and Sensitivity Analysis

4.3.1. Impact of individual algorithmic components

Component-wise ablation quantifies individual contributions to overall performance improvement. Removing neural parameter prediction while retaining adaptive mechanisms reduces energy savings from 31.7% to 22.3%, highlighting the importance of learned initialization. Disabling adaptive learning rates while keeping neural prediction decreases savings to 24.8%, demonstrating the value of dynamic parameter adjustment. Complete removal of learning components, reverting to standard convex optimization, yields only 15.2% improvement over heuristics.

The neural network architecture ablation explores depth and width impacts on prediction accuracy. Reducing hidden layers from five to three increases parameter prediction error by 18.4% and convergence iterations by 12.7%. Halving layer widths degrades performance by 9.2% while reducing inference time by 34%. The full architecture represents an effective trade-off between prediction quality and computational overhead. Feature importance analysis using SHAP values identifies workload autocorrelation (23.4%), resource requirement variance (19.8%), and arrival rate (17.2%) as most influential inputs.

Table 6: Ablation Study Results

Configuration	Energy Savings	Convergence Iterations	Inference Time (ms)	Training Time (hours)
Full System	31.7%	92.3	3.3	18.4
No Neural Prediction	22.3%	147.2	0.0	0.0
No Adaptive Rates	24.8%	118.6	3.3	18.4
No Momentum Adaptation	27.4%	106.1	3.3	18.4
Fixed Penalties	28.9%	98.7	3.3	18.4
Shallow Network (3 layers)	26.2%	104.3	2.1	8.7

Narrow Network (50% width)	28.6%	99.8	2.2	11.2

4.3.2. Robustness to parameter variations and workload changes

Sensitivity analysis evaluates algorithm robustness to parameter perturbations and workload distribution shifts. Learning rate base value variations (±50%) impact convergence speed but maintain solution quality within 3.2% of optimal. Momentum coefficient ranges (0.7-0.95) show stable performance with gradual degradation outside the recommended range. Penalty parameter bounds affect constraint satisfaction rates, with lower bounds risking violations and upper bounds causing numerical difficulties.

Workload distribution shifts test generalization capability beyond training data characteristics. Synthetic perturbations increasing task arrival variance by 100% reduce energy savings from 31.7% to 27.3%, demonstrating graceful degradation. Introducing new task types absent from training data decreases performance by 8.4% while maintaining constraint satisfaction. The system adapts to gradual distribution changes through online parameter updates, recovering 65% of performance loss within 100 iterations.

Scalability experiments vary problem dimensions to assess computational complexity scaling. Problem sizes from 100 to 10,000 tasks show sub-linear growth in solution time, achieving O(n^1.4) empirical complexity compared to O(n^2) for traditional solvers. Memory consumption scales linearly with problem size, requiring 8.3 MB per 1000 tasks. The largest tested instance with 10,000 tasks and 500 servers solves in 47.2 seconds while maintaining 28.9% energy improvement over baselines.

Cross-validation across different data center configurations validates transferability. Models trained on homogeneous server farms achieve 24.6% energy savings when deployed to heterogeneous environments. Configuration differences in server power profiles reduce savings by average 5.8% compared to matched training scenarios. Transfer learning with 10% target domain data recovers 82% of performance gap, suggesting effective adaptation strategies for deployment across diverse infrastructure.

5. Conclusions and Future Directions

5.1. Summary of Key Findings and Contributions

5.1.1. Achieved improvements in energy efficiency and convergence

This research demonstrates that integrating neural learning with convex optimization achieves significant advances in cloud resource scheduling efficiency. The experimental results confirm 31.7% average energy reduction across diverse workload patterns while accelerating convergence by 60.7% compared to traditional optimization methods. The approach successfully balances theoretical rigor with practical efficiency, maintaining mathematical convergence guarantees while adapting to dynamic workload characteristics. The learned parameter initialization reduces optimization iterations from 234.7 to 92.3 on average, translating to 54.4% computation time reduction despite neural network inference overhead.

5.1.2. Theoretical guarantees and practical applicability

The framework preserves convexity properties throughout the optimization process, ensuring global optimality within the convex formulation. KKT conditions provide verifiable optimality certificates, distinguishing this approach from purely heuristic methods lacking theoretical foundations. The proven convergence properties guarantee solution quality while adaptive mechanisms improve practical performance. Real-world deployment feasibility is validated through extensive testing on production workload traces, demonstrating robustness across varying operational conditions and scalability to cloud-scale problems involving thousands of servers and tasks.

5.2. Limitations and Open Challenges

5.2.1. Scalability considerations for large-scale deployments

Current implementation faces computational challenges when scaling beyond 10,000 concurrent tasks, primarily due to quadratic memory requirements for constraint matrices. The neural network inference time, though minimal at 3.3 milliseconds, accumulates significantly in systems requiring millisecond-level scheduling decisions. Distributed optimization strategies could address these limitations through problem decomposition and parallel processing. The training data requirements pose additional challenges,

necessitating extensive historical records that may not exist for novel workload types or newly deployed infrastructure.

5.3. Future Research Opportunities

5.3.1. Extension to non-convex problems through convex relaxation

Non-convex cloud optimization problems involving discrete server selection and nonlinear cooling dynamics present opportunities for extending the framework. Convex relaxation techniques such as semidefinite programming could approximate non-convex objectives while maintaining solution quality bounds. The learning component could predict effective relaxation parameters, tightening approximation gaps through data-driven insights. Sequential convex programming approaches iteratively refining solutions offer pathways to handle non-convexities while preserving convergence guarantees.

5.3.2. Integration with federated learning for distributed clouds

Federated learning enables collaborative model training across geographically distributed data centers without centralizing sensitive operational data. Privacy-preserving aggregation protocols could combine local learning insights while protecting proprietary information. The distributed training paradigm aligns with edge computing trends, enabling optimization models adapted to regional workload characteristics and infrastructure configurations. Asynchronous federated updates could accommodate varying network latencies and computational capabilities across participating sites, creating a globally optimized yet locally adapted resource management framework.

References

[1]. Asim, M., Wang, Y., Wang, K., & Huang, P. Q. (2020). A review on computational intelligence techniques in cloud and edge computing. IEEE Transactions on Emerging Topics in Computational Intelligence, 4(6), 742-763.

[2]. Hou, S., Ni, W., Zhao, S., Cheng, B., Chen, S., & Chen, J. (2020). Decentralized real-time optimization of voltage reconfigurable cloud computing data center. IEEE Transactions on Green Communications and Networking, 4(2), 577-592.

[3]. Yuan, H., & Zhou, M. (2020). Profit-maximized collaborative computation offloading and resource allocation in distributed cloud and edge computing systems. IEEE Transactions on Automation Science and Engineering, 18(3), 1277-1287.

[4]. Liu, J., Xiong, K., Ng, D. W. K., Fan, P., Zhong, Z., & Letaief, K. B. (2020). Max-min energy balance in wireless-powered hierarchical fog-cloud computing networks. IEEE Transactions on Wireless Communications, 19(11), 7064-7080.

[5]. Vu, T. T., Nguyen, D. N., Hoang, D. T., Dutkiewicz, E., & Nguyen, T. V. (2021). Optimal energy efficiency with delay constraints for multi-layer cooperative fog computing networks. IEEE Transactions on Communications, 69(6), 3911-3929.

[6]. Karatalay, O., Psaromiligkos, I., & Champagne, B. (2022). Energy-efficient resource allocation for D2D-assisted fog computing. IEEE Transactions on Green Communications and Networking, 6(4), 1990-2002.

[7]. Kopras, B., Bossy, B., Idzikowski, F., Kryszkiewicz, P., & Bogucka, H. (2022). Task allocation for energy optimization in fog computing networks with latency constraints. IEEE Transactions on Communications, 70(12), 8229-8243.

[8]. Wang, S., Li, X., & Gong, Y. (2023). Energy-efficient task offloading and resource allocation for delay-constrained edge-cloud computing networks. IEEE Transactions on Green Communications and Networking, 8(1), 514-524.

[9]. Tong, Z., Cai, J., Mei, J., Li, K., & Li, K. (2023). Computation offloading for energy efficiency maximization of sustainable energy supply network in IIoT. IEEE Transactions on Sustainable Computing, 9(2), 128-140.

[10]. Du, J., Xu, M., Gill, S. S., & Wu, H. (2023). Computation energy efficiency maximization for intelligent reflective surface-aided wireless powered mobile edge computing. IEEE Transactions on Sustainable Computing, 9(3), 371-385.

[11]. Pang, S., He, X., Hsu, C. H., Rong, C., Zhu, H., & Zhang, P. (2023). Joint trajectory and energy consumption optimization based on UAV wireless charging in cloud computing system. IEEE Transactions on Cloud Computing, 11(4), 3426-3438.

[12]. Hossain, M. A., & Ansari, N. (2023). Hybrid multiple access for network slicing aware mobile edge computing. IEEE Transactions on Cloud Computing, 11(3), 2910-2921.

[13]. Zhang, W., Zhang, Z., Zeadally, S., Chao, H. C., & Leung, V. C. (2020). Energy-efficient workload allocation and computation resource configuration in distributed cloud/edge computing systems with

stochastic workloads. IEEE Journal on Selected Areas in Communications, 38(6), 1118-1132.

[14]. Wilkes, J. (2020). Google cluster-usage traces v3 [Technical report]. Google Inc. https://github.com/google/cluster-data/blob/master/ClusterData2019.md